Crystallization Kinetics, Melting Behavior, and Morphologies of Poly(butylene succinate) and Poly(butylene succinate)-*block*-poly(propylene glycol) Segmented Copolyester

Xi Huang,[1,2] Chuncheng Li,[1] Guohu Guan,[1] Dong Zhang,[1] Yaonan Xiao[1]

[1]*Beijing National Laboratory for Molecular Sciences, CAS Key Laboratory of Engineering Plastics, Joint Laboratory of Polymer Science and Materials, Institute of Chemistry, Chinese Academy of Sciences, Beijing 100190, People's Republic of China*
[2]*Graduate University of the Chinese Academy of Sciences, Beijing 100049, People's Republic of China*

Received 3 November 2009; accepted 12 April 2010
DOI 10.1002/app.32585
Published online 11 June 2010 in Wiley InterScience (www.interscience.wiley.com).

ABSTRACT: This article investigated the crystallization kinetics, melting behavior, and morphologies of poly(butylene succinate)(PBS) and its segmented copolyester poly(butylene succinate)-*block*-poly(propylene glycol)(PBSP) by means of differential scanning calorimetry, polarized light microscopy, and wide angle X-ray diffraction. Avrami equation was used to describe the isothermal crystallization kinetics. For nonisothermal crystallization studies, the Avrami equation modified by Jeziorny, and the model combining Avrami equation and Ozawa equation were employed. The results showed that the introduction of poly(propylene glycol) soft segment led to suppression of crystallization of PBS hard segment. The melting behavior of the isothermally and nonisothermally crystallized samples was also studied. Results showed that the isothermally crystallized samples exhibited two melting endotherms, whereas only one melting endotherm was shown after nonisothermal crystallization. The spherulitic morphology of PBSP and wide angle X-ray diffraction showed that the polyether segments were excluded from the crystals and resided in between crystalline PBS lamellae and mixed with amorphous PBS. © 2010 Wiley Periodicals, Inc. J Appl Polym Sci 118: 2225–2235, 2010

Key words: crystallization kinetics; melting behavior; morphology

INTRODUCTION

Nowadays, universal use of nondegradable plastic products has caused serious environmental pollution. Developing biodegradable polymers becomes necessary and important to solve the problem. It is well-known that aliphatic polyesters are the most promising biodegradable polymers. Among aliphatic polyesters, poly(butylene succinate)(PBS) has relative high-melting temperature and other excellent properties. However, the insufficient mechanical properties of PBS, especially the poor impact strength, have prevented it from being used in diverse applications,[1,2] so various techniques[3–9] have been explored to improve these weaknesses. Among these researches, introducing polyether as soft segments into the polymer chain of PBS is an important way to improve impact strength of PBS.[6–9] The synthesized thermoplastic elastomer had satisfactory thermal, mechanical properties, and good biodegradability.

It is well-known that mechanical properties and biodegradability of polymer are affected by many factors, such as chemical composition, molecular weight, molecular weight distribution, crystal structure, and morphology.[10–13] Therefore, study on the crystallization behavior and morphology of polymer is useful to understand their effect on the properties.

Much attention has been paid to crystal structure, crystallization behavior, and melting behavior of PBS homopolymer.[14–18] For example, Ihn et al.[15] investigated the morphology, the lamellae thickness of PBS single crystals grown from solutions. Yoo and Im[16] studied the melting behavior of isothermally crystallized PBS. Yasuniwa and Satou,[18] presented the melting behavior of nonisothermally crystallized PBS by DSC.

However, there is a lack of information concerning the crystallization behavior of segmented copolyesters based on PBS as hard segment. Only a few studies of segmented copolymers based on terephthalic polyester [e.g., poly(ethylene terephthalate)] and polyether were published.[19–25] In these articles, the copolymers have been identified as semicrystalline-like materials, possessing crystalline polyesters and

Correspondence to: C. Li (lizy@iccas.ac.cn).
Contract grant sponsor: National High Technology Research and Development Program of China; contract grant number: 2009AA033601.

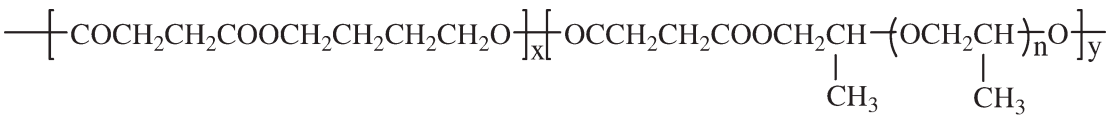

PBSP

PBS

Scheme 1 Chemical structure of PBSP and PBS.

well-mixed amorphous polyether and polyester domains. Ho et al.[24] synthesized low-ether-content poly(ester-ether)s with amide linkages. A crystallization mechanism through a heterogeneous nucleation process with homogeneous lamellar branching was proposed on the basis of the morphological observations and Avrami analysis.

In our previous article,[26] we successfully synthesized poly(butylene succinate)-*block*-poly(propylene glycol) (PBSP) segmented copolyesters with high-molecular weight based on PBS as the hard segments and PPG as the soft segments. The chemical structure for PBSP and PBS is shown in Scheme 1. The copolymers own excellent flexibility and biodegradability. As our proceeding study, this article attempted to investigate the effects of noncrystallizable segments on the crystallization kinetics, melting behavior, and morphology of segmented copolymer materials. It is well-known that macroscopic segregation may happen in high-ether-content segmented copolyester. Therefore, copolyester(PBSP) with low PPG content(10 mass%) was chosen as the sample. The molecular weight of PPG was 1000 g mol^{-1} in this article.

EXPERIMENTAL

Materials

PBSP and PBS, for the investigation, were synthesized by two-step melt polycondensation. Take the polymerization process of PBSP for example. In the first esterification step, 62.9 g of succinic acid (SA) and 79.2 g of 1,4-butanediol (BD) were introduced into a 500 mL, four-necked flask equipped with a mechanical stirrer, a thermometer and a nitrogen inlet tube. The reactor was heated under nitrogen atmosphere at 180°C, and held there until theoretical amount of water was removed. In the second step, 18.4 g of poly(propylene glycol), 0.15 mL titanium (IV) butoxide as catalyst were added to the reaction system. The pressure of the reaction system was gradually reduced to 10–15 Pa. The temperature was raised to 220–230°C and maintained at this temperature for 3–8 h. As the polymerization was finished, nitrogen was introduced into the reaction system and normal pressure was returned so that the obtained copolyester can be taken out. They were purified by reprecipitation from chloroform solution by methanol repeatedly, and then they were dried in a vacuum oven for 10 h at 80°C. The description of the materials is shown in Table I.

The chemical structure and composition of copolyester were confirmed by means of ^{1}H-NMR. The intrinsic viscosities of the polymers were measured in a Ubbelohde viscometer at a concentration of 1 g dL^{-1} with metacresol as solvent. The temperature was kept at 25 ± 0.1°C. The molecular weight and molecular weight distribution were determined by gel permeation chromatography (Waters 2695 GPC, MA) at 35°C. The eluent was chloroform at a flow

TABLE I
Composition, Molecular Weight, Intrinsic Viscosity, and Thermal Parameters of PBS and PBSP

	Mass fraction of soft segments (%)								
Sample	Feed	Found	[η] (dL g^{-1})	M_n (×10^4 g mol^{-1})	M_w (×10^4 g mol^{-1})	M_w/M_n	T_g[a] (°C)	T_m[b] (°C)	T_c[c] (°C)
PBS	–	–	1.11	6.2	12.1	1.96	−44.2	111.4	66.0
PBSP	10	8.74	1.24	7.6	19.2	2.53	−46.6	108.0	56.9

[a] Glass transition temperature defined by the mid-point of heat capacity change between the glass and melt.
[b] Melting temperature defined by the peak maximum for the endotherm on second heat.
[c] Temperature of maximum crystallization rate defined by the exotherm peak maximum on cool.

rate of 1.0 mL min^{-1}. The molecular weights and the molecular weight distributions were calculated against polystyrene standards.

The basic thermal parameters were determined by differential scanning calorimetry (Perkin-Elmer diamond DSC) under high-purity nitrogen gas condition, and the calibration of temperature was performed using indium as standard before the measurements. All of the samples were heated to 150°C and held there for 5 min to erase thermal history before they were cooled to −100°C as soon as possible. After that, they were heated to 150°C at a rate of 20°C min^{-1} and then cooled to −100°C at the same rate. The endothermic and exothermic curves were recorded to determine the thermal parameters.

Differential scanning calorimetry (DSC) procedures

Isothermal, nonisothermal crystallization kinetics, and melting behavior studies were carried out using a Perkin-Elmer DSC-7. The instrument was calibrated using indium before the measurements. Crystallization temperatures were calibrated by extrapolation of the melting temperature of indium to zero heating rate. All the measurements were conducted under a high-purity nitrogen atmosphere. The weight of sample was about 5 mg.

The isothermal crystallization studies were performed as follows: the samples sealed in aluminum pan were heated to 150°C and held there for 5 min to erase any thermal history, and then cooled to the designated crystallization temperature(T_c) at a rate of 200°C min^{-1} for isothermal crystallization. The exothermal curves of heat flow as a function of time were recorded for isothermal crystallization studies. After the crystallization was completely finished, the isothermally crystallized samples were heated directly from T_c to 150°C at a rate of 20°C min^{-1}. The endothermal curves were recorded to analyze the melting behavior.

For nonisothermal crystallization studies, the samples were heated to 150°C and held there for 5 min to eliminate any thermal or mechanical history before cooling the melt to crystallize at different cooling rates. The curves of heat flow as a function of temperature were recorded. The cooling rates used in this study were 5, 8, 10, 15, and 20°C min^{-1}, respectively.

Polarized light microscopy (PLM)

The morphologies of the polymers after melt-crystallization at the stated temperature were examined with PLM (Olympus DX51). The ultrathin film was prepared on the cover glass by solution cast method. Before observation, the film was heated to 150°C and kept there for 5 min to eliminate any thermal history, and then it was cooled rapidly to the designated temperature for isothermal crystallization.

Wide angle X-ray diffraction (WAXD)

WAXD measurements were carried out at room temperature with a Ragaku Model D/max-2B diffractometer system using Cu–Kα radiation (40 KV, 200 mA); testing data were collected from 2 to 40° at a scanning rate of 2° min^{-1}. The samples were prepared by the following ways. The PBS and PBSP sheets were preheated at 130°C for 10 min to erase the thermal and mechanical history. After that, the polymer sheets were cooled rapidly to the isothermal crystallization temperature. After crystallization at 78°C for 10 min, the samples were used for wide angle X-ray diffraction characterizations, respectively.

RESULTS AND DISCUSSION

Isothermal crystallization analysis

The exothermic crystallization curves of polymers at various crystallization temperatures (T_c) are shown in Figure 1. It can be seen that for both of the two samples, the curves became flatter and the crystallization exothermic peak gradually shifted to longer time with increasing T_c. This indicated that the isothermal crystallization process took more time to approach the final equilibrium state. Besides, the incorporation of PPG soft segment in PBS results in longer time to reach the equilibrium state at the same T_c.

To investigate the isothermal crystallization kinetics in detail, the well-known Avrami equation[27,28] was employed.

The expression for the equation is as follow:

$$X(t) = 1 - \exp(-Kt^n) \quad (1)$$

where $X(t)$ is the relative degree of crystallinity, which can be calculated as the ratio of the area of the exothermal peak at time t to the total measured area of crystallization, t is the crystallization time, K is the crystallization rate constant that contains the crystal geometry, nucleation, and crystal growth rate, n is the Avrami exponent determined by nucleation mechanism and the crystal geometry. The Avrami equation could be further deduced as

$$\lg\{-\ln[1 - X(t)]\} = n \lg t + \lg K \quad (2)$$

Thus the Avrami parameters (n and K) at each isothermal crystallization temperature T_c can be

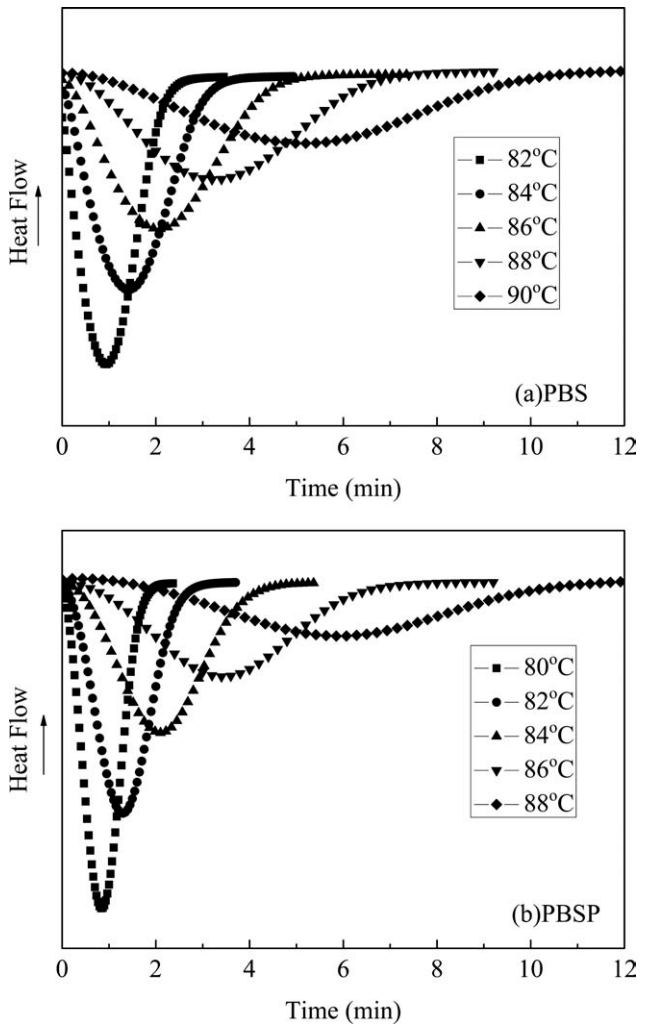

Figure 1 Heat flow as a function of time during isothermal crystallization at different crystallization temperatures by DSC for (a) PBS and (b) PBSP.

determined from the linear plots of lg{-ln[1- $X(t)$]} against lg$t$ as shown in Figure 2.

It can be seen that, all the curves showed an initial linear portion and then deviated from the straight line at the later stage. This trend was attributed to a primary crystallization followed by a secondary crystallization process. The values of n and K determined from the initial linear section in Figure 2 are listed in Table II. The n value for PBS was little smaller than that of PBSP at the same isothermal crystallization temperature. This indicated that the crystal growth mechanism of PBSP might be different from that of PBS as the introduction of PPG soft segment. From the results in Table II, it could also be seen that the K values decreased with the increasing T_c for PBS and PBSP.

Figure 3 shows the relative degree of crystallinity versus crystallization time for PBS and PBSP. All the curves had sigmoidal shapes, which was typical of polymer crystallization behavior.

The value of half–time of crystallization ($t_{1/2}$) is another important parameter, which is defined as the time at which the relative degree of crystallinity is 50%. It can be obtained directly from Figure 3 or determined from the following equation:

$$t_{1/2} = (\ln 2/K)^{1/n} \tag{3}$$

where K and n are kinetic parameters. The values of $t_{1/2}$ obtained both from Figure 3 and eq. (3) are listed in Table II. We could see that the values derived from eq. (3) were in good agreement with those obtained from experimental figures. Usually, the rate of crystallization is described as the reciprocal of $t_{1/2}(1/t_{1/2})$. For both PBS and PBSP, the values of $1/t_{1/2}$ reduced with increasing crystallization temperature. That is to say, the crystallization rate slowed down. This is in agreement with the general conclusions obtained earlier.

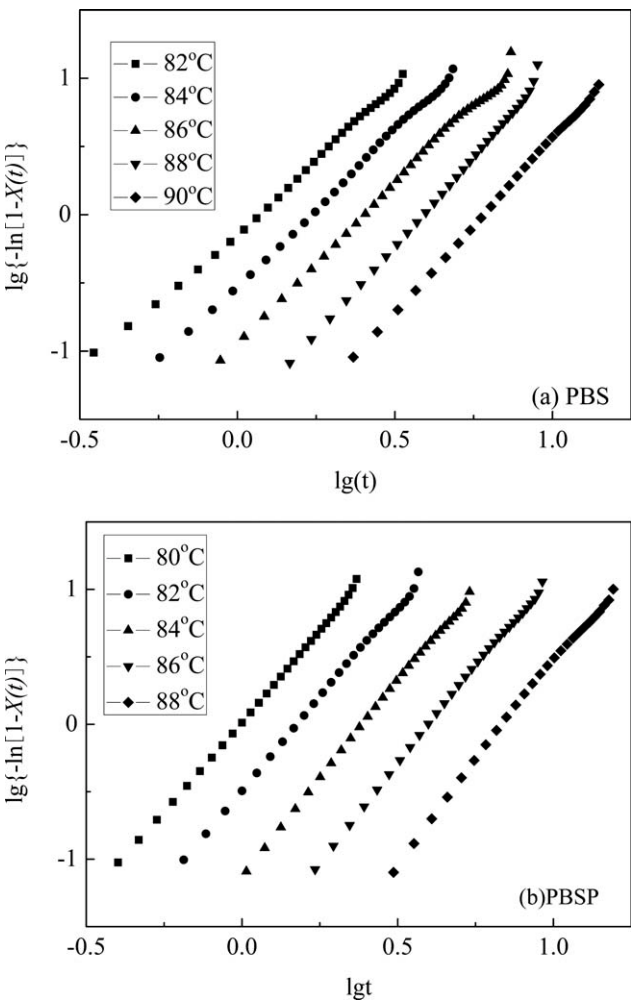

Figure 2 The plots of lg{-ln[1- $X(t)$]} versus lg$t$ for (a) PBS and (b) PBSP.

TABLE II
Kinetic Parameters of Isothermal Crystallization for PBS and PBSP

Sample	T_c(°C)	n	$K(\min^{-1/n})$	$t_{1/2}$ (min)[a]	$t_{1/2}$ (min)[b]
PBS	82	2.24	0.6944	0.999	0.994
	84	2.28	0.2930	1.459	1.476
	86	2.35	0.1134	2.158	2.176
	88	2.55	0.0309	3.380	3.390
	90	2.55	0.0103	5.230	5.260
PBSP	80	2.65	1.0505	0.855	0.864
	82	2.76	0.3267	1.313	1.318
	84	2.93	0.0746	2.142	2.140
	86	2.94	0.0175	3.500	3.498
	88	3.14	0.0024	6.048	6.033

[a] Determined from eq. (3).
[b] Obtained from Figure 3.

Nonisothermal crystallization analysis

Although most of the research work focused on the crystallization analysis of polymer under isothermal conditions, it is necessary and important to investigate the behavior of polymer during nonisothermal crystallization from the melt, because industrial processes generally proceed under nonisothernal environment. So, in the following section, we compare the nonisothermal crystallization properties of PBS and PBSP.

The nonisothermal crystallization exothermic curves of PBS and PBSP at various cooling rates (φ) are illustrated in Figure 4. T_p, the peak temperature, which corresponds to the maximum crystallization rate, shifted to lower temperature with increasing φ both for PBS and PBSP. It is also seen that the lower the cooling rate, the earlier the crystallization started. This observation is common for semicrystalline polymer crystallized nonisothermally.

In the nonisothermal crystallization, the time t has the relation with the temperature T as follows:

$$t = (T - T_0)/\varphi \tag{4}$$

where T is the temperature at time t, T_0 is the temperature at which the crystallization begins ($t = 0$), and φ is the cooling rate. As a result, the relative degree of crystallinity as a function of time (Fig. 5) can be given. All the curves showed S shape, which was consonant with the results of isothermal crystallization. Besides, the higher the cooling rate, the less the crystallization time.

Modified Avrami equation by Jeziorny

Mandelkern[29] considered that the Avrami equation can describe the primary stage of nonisothermal crystallization, based on the assumption that the crystallization temperature is constant. The following equation is obtained:

$$1 - X(t) = \exp[-Z_t t^n] \tag{5}$$

$$\lg\{-\ln[1 - X(t)]\} = n \lg t + \lg Z_t \tag{6}$$

where $X(t)$ is the relative degree of crystallinity at time t, Z_t is the rate constant in the nonisothermal

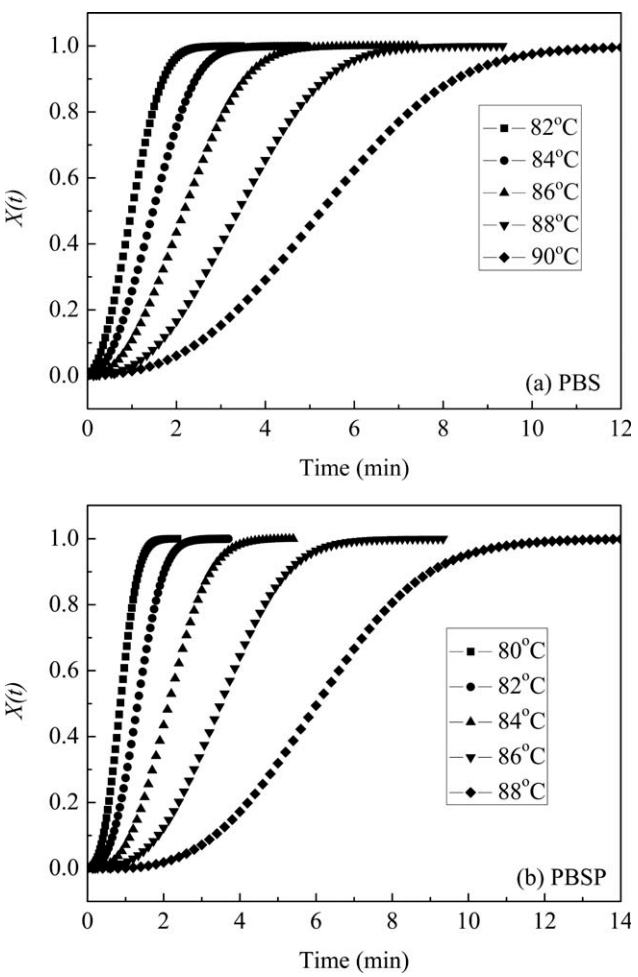

Figure 3 Relative degree of crystallinity as a function of time at various crystallization temperatures for (a) PBS and (b) PBSP.

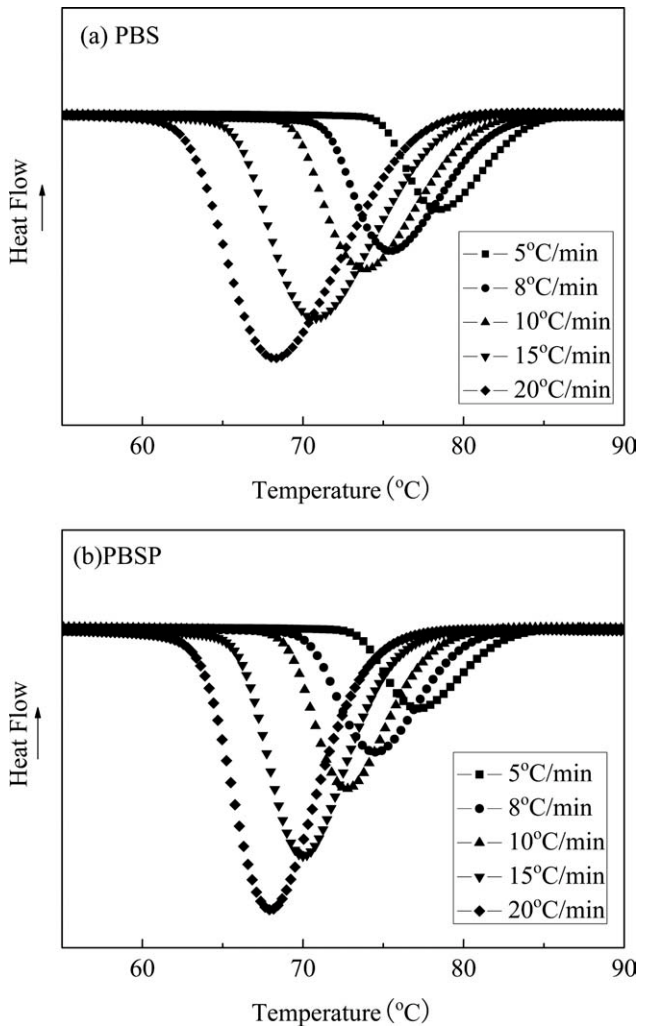

Figure 4 The DSC curves of (a) PBS and (b) PBSP, cooled from the melt at various cooling rates.

crystallization process. Considering the influence of the cooling or heating rate, Jeziorny[30] considered the values of Z_t should be inadequate, because of the influence of the cooling rate. Assuming that the cooling rate is constant or approximately constant, the final form of the Z_t characterizing the kinetics of nonisothermal crystallization was given as follows:

$$\log Z_c = \frac{\log Z_t}{\varphi} \tag{7}$$

As eq. (6) indicated, the values of n, Z_t can be obtained by the linear plots of lg{-ln[1- $X(t)$]} versus lg$t$ for PBS and PBSP, respectively. They are shown in Table III with the values of Z_c. It can be seen that the values of n for PBSP were larger than that of PBS, which indicated that the addition of PPG soft segment influences the mechanism of nucleation and the growth of PBS crystals. At the same time, the values of Z_c increased with increasing cooling rate for both PBS and PBSP. And the Z_c for PBSP was smaller than that of PBS at the same cooling rate. The existence of soft segment might hinder the crystallization under nonisothermal conditions.

Combined Avrami equation and Ozawa equation

To analysis the nonisothermal crystallization process exactly, the equation combining Avrami and Ozawa equation proposed by Mo and coworkers[31] was employed. The equations are described as follow:

$$n \ln t + \ln Z_t = \ln K_c - m \ln \varphi \tag{8}$$

$$\ln \varphi = (1/m) \ln[K_c/Z_t] - (n/m) \ln t \tag{9}$$

$$\ln \varphi = \ln F(T) - a \ln t \tag{10}$$

where $F(T) = [K_c/Z_t]^{1/m}$ and $a = n/m$. The rate parameter $F(T)$ has definite physical meaning. It refers to the necessary value of cooling rate to reach a defined degree of crystallinity at unit crystallization time. The smaller the value of $F(T)$, the higher the crystallization rate. At a given degree of crystallinity,

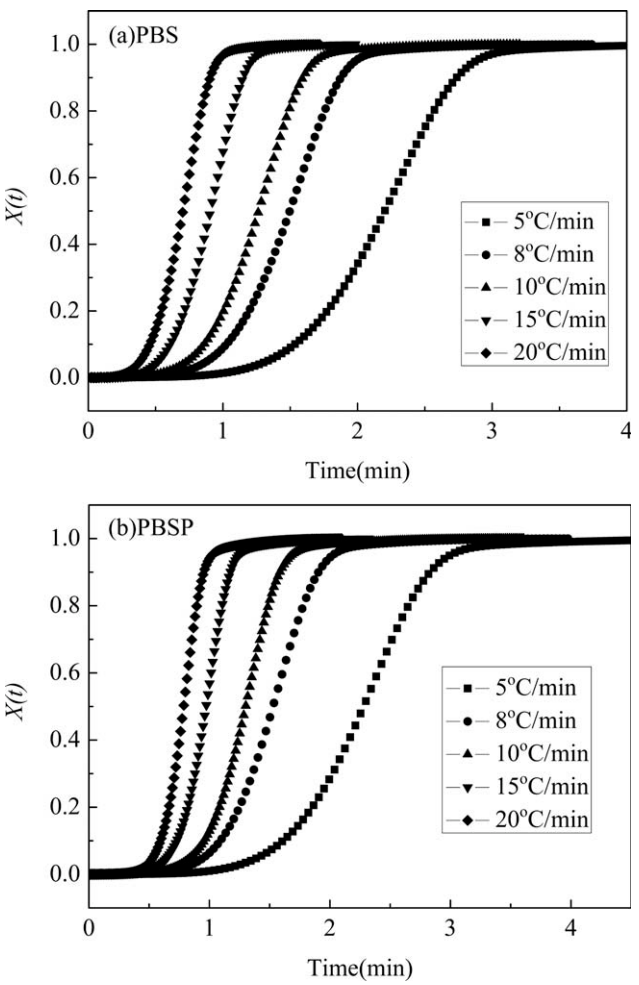

Figure 5 Relative degree of crystallinity as a function of time at various cooling rates for (a) PBS and (b) PBSP.

TABLE III
Nonisothermal Crystallization Kinetic Parameters of PBS and PBSP Based on Avrami Equation Modified by Jeziorny

Sample	φ(°C min^{-1})	*n*	Z_t	Z_c
PBS	5	5.19	0.0118	0.4114
	8	4.97	0.0957	0.7458
	10	4.79	0.2280	0.8626
	15	4.67	1.1054	1.0067
	20	4.22	2.9925	1.0563
PBSP	5	5.31	0.0088	0.3879
	8	5.33	0.0707	0.7180
	10	6.17	0.1365	0.8194
	15	6.48	0.8237	0.9872
	20	6.22	2.9670	1.0559

the plot of lnφ as a function of ln*t* gives a straight line with ln*F*(*T*) as the intercept and *-a* as the slope. The plots of lnφ versus ln*t* at various degree of crystallinity are shown in Figure 6. The good linearity of the plots verifies the advantage of the combined approach applied in this case. The values of *F*(*T*) and *a* are listed in Table IV. It can be seen that the value of *F*(*T*) increased with increasing relative degree of crystallinity for PBS and PBSP, respectively, indicating that a higher cooling rate was required to achieve a higher degree of crystallinity at unit crystallization time. However, at the same degree of crystallinity, the values of *F*(*T*) for PBS were all smaller than that of PBSP, which indicated that the crystallization rate of PBSP was lower compared with that of PBS under nonisothermal crystallization.

There are two possible ways to explain the slow-down phenomenon in the crystallization rate. First, it is the dilution effect for nucleation. The soft segments inevitably dilute the probability for nucleation and increase the energy barrier for nucleation, slowing down the crystallization. Second, the exclusion of the noncrystallizable component may lead to a change in the composition of the amorphous phase, changing its free energy in a manner dependent on the Flory interaction parameter. A possible consequence is that the change in the composition of the amorphous phase could lead to the phase separation or concentration gradient of the previously miscible phase. The formation of a phase boundary thus hinders the proceeding of crystallization. The hindering mechanism, called *soft impingement* by Cheng and Wunderlich,[32] has often been observed in copolymer systems.

Melting behavior following isothermal crystallization

The heat flow curves of PBS and PBSP after isothermal crystallization at different temperatures are shown in Figure 7. For both PBS and PBSP, multiple endothermic peaks during the heating were observed, which is common for semicrystalline polymer and their copolymer. The lower melting peak (T_L) shifted to higher temperatures with increasing isothermal crystallization temperature, whereas the position of higher melting peak (T_H) almost unchanged. However, the area of T_L increased but that of T_H decreased with increasing crystallization temperature. The phenomena can be ascribed to the melt-recrystallization process occurring during the DSC scan, which was explained in detail in our previous study.[33] The melting behavior of PBSP was similar to that of PBS, so that it also can be explained by the melt-recrystallization model. The melting peak in lower temperature was associated with the fusion of the metastable crystals grown by normal primary crystallization and the melting peak in higher temperature was the melting peak of the most perfect crystals after reorganization during the DSC measurement.

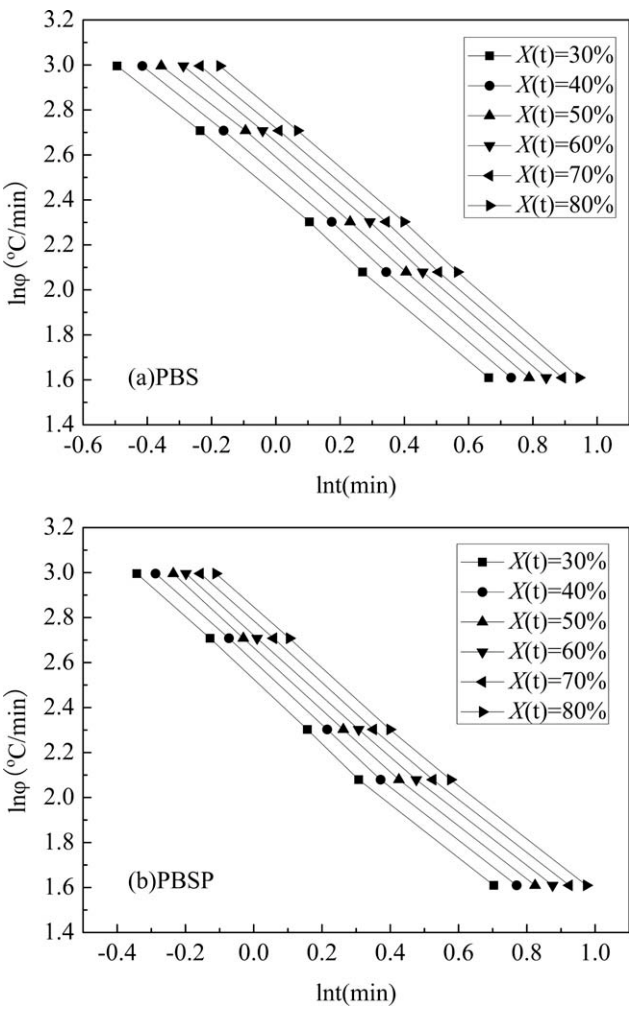

Figure 6 Plots of lnφ versus ln*t* based on the equation combining Avrami model and Ozawa model for (a) PBS and (b) PBSP.

TABLE IV
Nonisothermal Crystallization Kinetic Parameters of PBS and PBSP Based on Combined Avrami Model and Ozawa Model Analysis

	PBS				PBSP			
$X(t)$ (%)	$F(T)$	a	$(r^2)^a$	SD	$F(T)$	a	$(r^2)^a$	SD
30	11.17	1.21	0.999	0.01	12.50	1.34	0.998	0.03
40	12.21	1.21	1	0.01	13.50	1.32	0.998	0.03
50	13.15	1.22	0.999	0.01	14.39	1.31	0.998	0.03
60	14.16	1.23	1	0.01	15.18	1.30	0.998	0.02
70	15.08	1.23	1	0.01	16.08	1.29	0.998	0.02
80	16.23	1.24	1	0.01	17.08	1.28	0.999	0.02

SD is the standard variance.
[a] r^2 is the correlation coefficient of the line.

Melting behavior following nonisothermal crystallization

The heating curves of PBS and PBSP after nonisothermally crystallized at different cooling rates are shown in Figure 8. It is seen that, there is only one melting endothermic peak for both of the two samples. In the research of Yasuniwa and Satou,[18] Qiu et al.[17] and liu et al.,[33] it is reported that another lower endothermic peak or shoulder before higher endothermic peak during the heating process was observed, which was ascribed to the melt-recrystallization mechanism. However, this

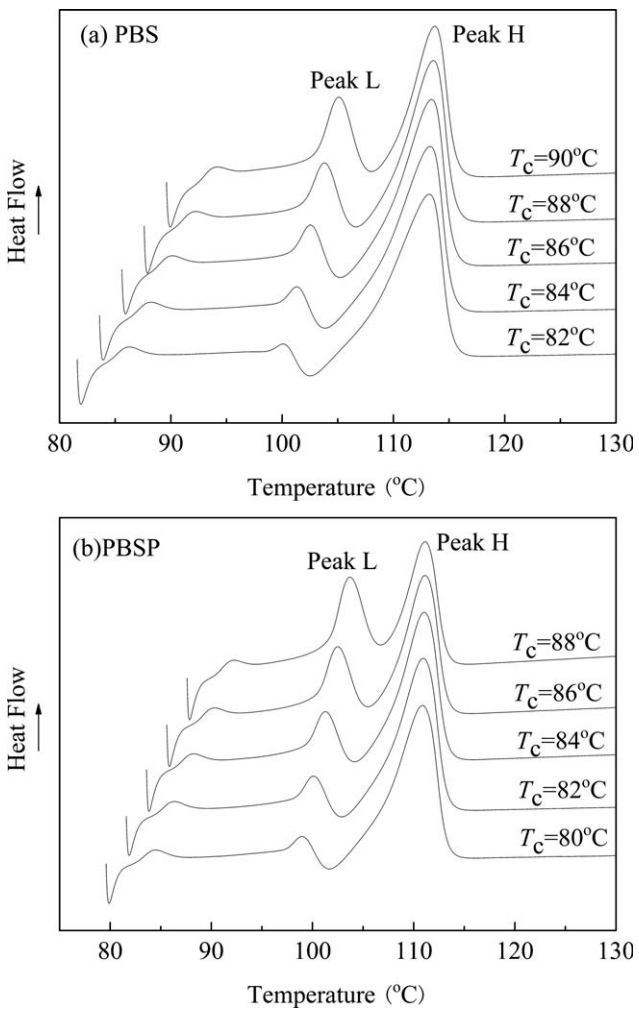

Figure 7 Melting curves after isothermal crystallization at different temperatures (a) PBS and (b) PBSP. Heating rate is 20°C min^{-1}.

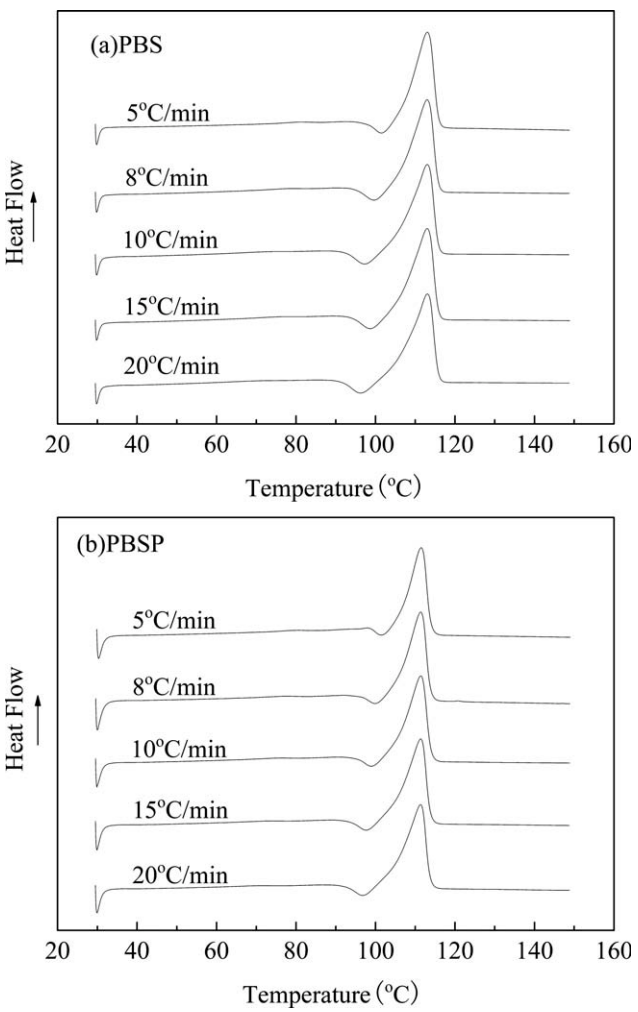

Figure 8 Melting curves for (a) PBS and (b) PBSP after nonisothermal crystallization at different rates. The heating rate was 20°C min^{-1}.

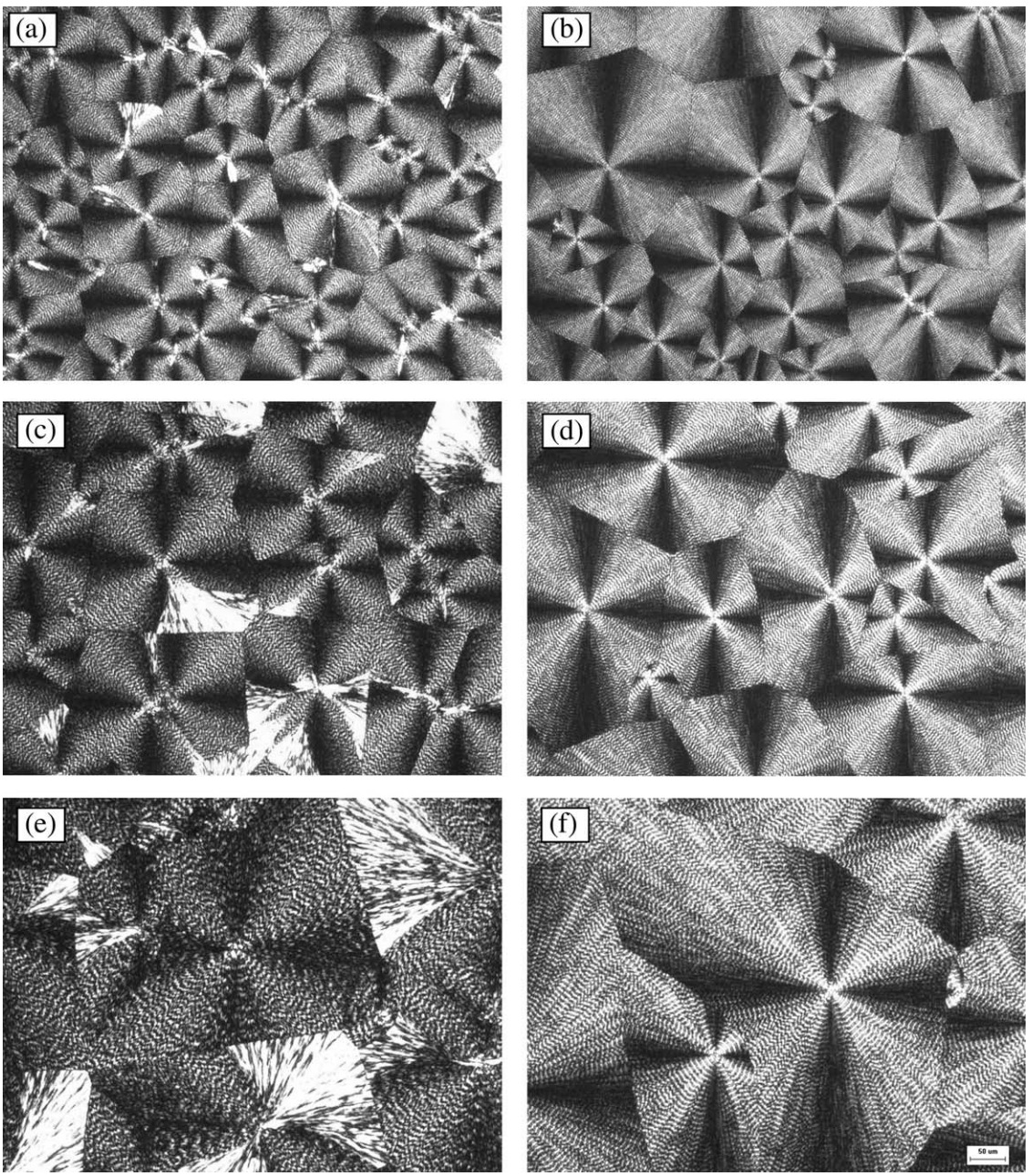

Figure 9 The spherulitic morphologies of PBS and PBSP after being crystallized isothermally at different temperatures; (a), (c), and (e) for PBS crystallized at 78, 82, and 86°C, respectively; (b), (d), and (f) for PBSP crystallized at 78, 82, and 86°C, respectively. All the pictures have the same scale.

phenomenon was not observed in our experiment, which may be caused by the difference in sample and experiment conditions. Besides, an exothermic peak was found before the endothermic peak. And the temperature of the exothermic peak decreased with increasing cooling rate. The results indicated that fusion and recrystallization were competitive in the heating process. The primary crystallites formed during nonisothermal melt-crystallization were not stable enough and, upon subsequent heating process, the rate of recrystallization exceeded that of the fusion.

Morphological observations

After the samples crystallized isothermally at different temperatures, morphologies of PBS and PBSP are illustrated in Figure 9.

As shown in Figure 9, PBS and PBSP both show typical spherulitic morphology under crossed polarizer. These spherulites grow radially and finally impinge against each other, therefore, linear boundary between neighboring spherulites was observed.

In addition to typical Maltese cross, ringed extinction patterns were observed and the band spacing

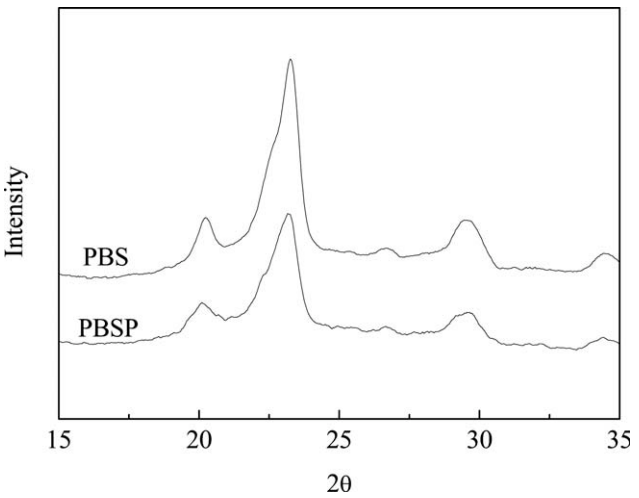

Figure 10 WAXD patterns of PBS and PBSP. The samples crystallized at 78°C for 10 min.

increased with the increasing crystallization temperature T_c. This phenomenon was common in many crystalline polymers. The periodic extinction of banded spherulite was caused by lamella twist during growth, and the increase in band space was related to the bigger layer thickness of lamella formed at a higher T_c.[34] For PBS, as the crystallization temperature increased, the ringed bands in some parts of the spherulites disappeared. This may be caused by the weaker inherent strains between lamellar crystals which prevents the twisting of ringed lamellar crystals.[35]

Considering the component of copolyester, the soft segment is noncrystallizable, whereas the hard segment is crystallizable, and they are connected by chemical bonds, so it is interesting to investigate the state of the two parts in the crystal structure. Up to now, there are two models for crystallization of dissimilar chains. Crystallizable segments may form crystal structure of their own with excluding out the alien segment. They also may co-crystallize different segments to form co-crystals or crystals with defects. The former is exclusion model and the latter is inclusion model.[36] For the size of soft segment, exclusion model should be most likely the consequence. The crystal structures of PBS and the segmented copolyester were characterized by X-ray diffraction. Figure 10 shows the WAXD patterns of the PBS and PBSP. It can be seen that the pattern of PBSP shows similar diffraction peaks with that of PBS, suggesting that the crystal structure of PBSP is almost the same as that of PBS. On the basis of the result, it indicates that the PPG soft segments exist in amorphous region and are excluded from the crystalline region, which is composed of PBS hard segment. The lamellar model is close to the exclusion model.

CONCLUSIONS

The crystallization kinetics, melting behavior, and morphologies of PBS and PBSP were studied in detail in this article. Based on isothermal and nonisothermal crystallization investigation, the introduction of PPG soft segment lead to lower crystallization rate for PBSP compared with that of PBS. Double melting endothermic peaks were found on crystallized PBS and PBSP at various isothermal temperatures, which was explained by melt-recrystallization mechanism. But this phenomenon was not clearly observed during the melting process following nonisothermal crystallization. According to morphological observations and WAXD result, PBSP crystallized with typical spherulitic morphology and PPG soft segment resided in between the PBS lamellas after exclusion from PBS crystals.

References

1. Kasuya, K. I.; Takagi, K. I.; Ishiwatari, S. I.; Yoshida, Y.; Doi, Y. Polym Degrad Stab 1998, 59, 327.
2. Nagata, M.; Kiyotsukuri, T.; Minami, S.; Tsutsumi, N.; Sakai, W. Polym Int 1996, 39, 83.
3. Cao, A.; Okamura, T.; Ishiguro, C.; Nakayama, K.; Inoue, Y.; Masuda, T. Polymer 2002, 43, 671.
4. Chae, H. G.; Park, S. H.; Kim, B. C.; Kim, D. K. J Polym Sci Part B: Polym Phys 2004, 42, 1759.
5. Jin, H. J.; Lee, B. Y.; Kim, M. N.; Yoon, J. S. J Polym Sci Part B: Polym Phys 2000, 38, 1504.
6. Nagata, M.; Kiyotsukuri, T.; Takeuchi, S.; Tsutsumi, N.; Sakai, W. Polym Int 1997, 42, 33.
7. Pepic, D.; Zagar, E.; Zigon, M.; Krzan, A.; Kunaver, M.; Djonlagic, J. Eur Polym J 2008, 44, 904.
8. Petic, D.; Nikolic, M. S.; Djonlagic, J. J Appl Polym Sci 2007, 106, 1777.
9. Lee, S. I.; Yu, S. C.; Lee, Y. S. Polym Degrad Stab 2001, 72, 81.
10. Kint, D. P. R.; Alla, A.; Deloret, E.; Campos, J. L.; Guerra, S. M. Polymer 2003, 44, 1321.
11. Witt, U.; Müller, R. J.; Deckwer, W. D. Macromol Chem Phys 1996, 197, 1525.
12. Cho, K.; Lee, J.; Kwon, K. J Appl Polym Sci 2001, 79, 1025.
13. Koyama, N.; Doi, Y. Macromolecules 1997, 30, 826.
14. Ichikawa, Y.; Kondo, H.; Igarashi, Y.; Noguchi, K.; Okuyama, K.; Washiyama, J. Polymer 2000, 41, 4719.
15. Ihn, K. J.; Yoo, E. S.; Im, S. S. Macromolecules 1995, 28, 2460.
16. Yoo, E. S.; Im, S. S. J Polym Sci Part B: Polym Phys 1999, 37, 1357.
17. Qiu, Z. B.; Komura, M.; Ikehara, T.; Nishi, T. Polymer 2003, 44, 7781.
18. Yasuniwa, M.; Satou, T. J Polym Sci Part B: Polym Phys 2002, 40, 2411.
19. Cella, R. J. J Polym Sci Polym Symp 1973, 42, 727.
20. Shen, M.; Mehra, U.; Niinomi, M.; Koberstein, J. T.; Cooper, S. L. J Appl Phys 1974, 45, 4182.
21. Seymour, R. W.; Overton, J. R.; Corley, L. S. Macromolecules 1975, 8, 331.
22. Lilaonitkul, A.; West, J. C.; Cooper, S. L. J Macromol Sci Phys 1976, 12, 563.
23. Zhu, L. L.; Wegner, G. Macromol Chem Phys 1981, 182, 3625.

24. Ho, R. M.; Hseih, P. Y.; Yang, C. C.; Lin, J. J. J Polym Sci Part B: Polym Phys 2001, 39, 2469.
25. Ho, R. M.; Chi, C. W.; Tsai, C. C.; Lin, J. J. Polymer 2002, 43, 1365.
26. Huang, X.; Li, C. C.; Zheng, L. C.; Zhang, D.; Guan, G. H.; Xiao, Y. N. Polym Int 2009, 58, 893.
27. Avrami, M. J Chem Phys 1939, 7, 1103.
28. Avrami, M. J Chem Phys 1940, 8, 212.
29. Mandelkern, L. Methods of Experimental Physics, Part B; Academic Press: New York, 1980.
30. Jeziorny, A. Polymer 1978, 19, 1142.
31. Liu, J. P.; Mo, Z. S.; Qi, Y. C.; Zhang, H. F.; Chen, D. L. Acta Polym Sin 1993, 1, 1.
32. Cheng, S. Z. D.; Wunderlich, B. Macromolecules 1988, 21, 3327.
33. Liu, X. Q.; Li, C. C.; Zhang, D.; Xiao, Y. N. J Polym Sci Part B: Polym Phys 2006, 44, 900.
34. Bassett, D. C. Principles of Polymer Morphology; Cambridge University Press: Cambridge, 1981.
35. Gan, Z. H.; Abe, H.; Doi, Y. Biomacromolecules 2001, 2, 313.
36. Cheng, S. Z. D.; Janimak, J. J.; Zhang, A.; Hsieh, E. T. Polymer 1991, 32, 648.